PFC/JA-87-17

Experimental Study of Nonlinear M=1 Modes in the Tara Tandem Mirror

J.H. Irby, B.G. Lane, J.A. Casey, K. Brau,
S.N. Golovato, W.C. Guss, S.F. Horne,
J. Kesner, R.S. Post, E. Sevillano
J.D. Sullivan, and D.K. Smith

April 1987

Plasma Fusion Center
Massachusetts Institute of Technology
Cambridge, Massachusetts 02139 USA

Submitted for publication in: The Physics of Fluids.

This work was supported by Department of Energy Contract No. DE-AC02-78ET51013.

ABSTRACT

The nature of a rigid, flute-like $M = 1$ instability as seen in the Tara tandem mirror is discussed. Radial density and light emission profiles obtained by inverting chord measurements are compared to endloss radial profiles during the evolution of the mode to its non-linear saturated state. This final state is characterized by a coherent, flute-like motion of the plasma as a whole about the machine axis. No evidence for trapped particle modes has been found.

INTRODUCTION

In this paper we report on the details of an $M = 1$ instability as seen in the Tara tandem mirror[1,2]. Modes similar to the one reported here have been documented on the TMX, Phaedrus, and HIEI mirror experiments[3-7], as well as on earlier mirror machines[8,9].

A schematic of the Tara experiment is shown in Figure 1. The experiment consists of an axisymmetric central cell bounded on both ends by axisymmetric plugs and outboard minimum-B quadrupole anchors. In the work discussed in this paper, the plasma is not trapped in the anchors but free-streams through it (the anchor coils are energized only to preserve mapping to the endwall detectors). The plasma density and pressure is concentrated in the central cell which is purely axisymmetric. At the mid-plane of the central cell is a magnetic "hill" where the magnetic field rises to 4.6 kG from a value of 2.3 kG in the "wells" on either side. Located on the hill is a "slot" antenna which launches 300-500 kW of RF power resonant with the ion cyclotron frequency at the bottom of the wells[2]. This is the main power source for the central cell plasma. Also located on the hill is a gas box[10] which provides the fueling source for the machine and a ring-null divertor

which provides enhanced stability for the central cell plasma.

The plasma is initiated and sustained by the central cell slot antenna for 60 *msec*. The time history of several plasma parameters, including density, diamagnetism, and RF power sources is shown in Figure 2. The peak plasma density reached during a typical shot is $2.5 \times 10^{12}\ cm^{-3}$ with electron and ion temperatures of 80 to 100 eV and 600 to 800 eV, respectively. The peak beta in the central cell is 1%.

Since the central cell plasma is confined in an axisymmetric region without plasma pressure in the stabilizing anchor cells, it is expected theoretically to be unstable to magnetohydrodynamic interchange modes driven by unfavorable curvature and, in certain cases, to rotational modes driven by the plasma azimuthal rotation. Experimentally, however, there is a range in operating parameters in which a quiescent plasma can be sustained in Tara. The source of the stabilization is not yet clear, although ponderomotive effects due to the ion cyclotron heating (ICH) power[11-18] and edge stabilization effects due to interactions with limiters[19] have been investigated. A discussion of the stable operating parameter regime, and the extension of that

regime through the installation of a magnetic divertor, is the subject of another paper[20]. In this paper, we concentrate on the nature of the mode itself. The mode is usually initiated by the turn-on of the plug gyrotron (shown in Figure 2b), although it can be initiated by other power sources, as well as by adjustments of the gas fueling rates and slot antenna power level.

The organization of the paper is as follows: in section II we describe the diagnostic set that will be used in the subsequent analysis and in section III we examine the turn-on of the instability and present a model of the instability that is consistent with the diagnostic signals. In section IV we summarize our analysis.

II. Diagnostic Set

We summarize in this section the main diagnostics used in the analysis of the $M = 1$ mode.

Multi-chord interferometer array: A five chord interferometer array is mounted in the south mirror well. Chord radii of -6, -4, 0, 8, and 14 *cm* are used. The maximun size of the plasma at this location is determined by the limiter in the gas box. This limiter maps to

a radius of 19.5 cm at the array location. The $M = 1$ mode analysis of the multi-chord interferometer array assumes a Gaussian profile with ellipticity, offset, and coherent oscillation of the plasma column about the offset axis:

$$n_e(\mathbf{r}) = n_e \exp\left(- \frac{x'^2 + \epsilon y'^2}{r_0^2} \right), \qquad (1)$$

with x' and y' co-rotating with the plasma column:

$$x' = x \cos\theta + y \sin\theta \qquad \text{and} \qquad y' = y \cos\theta - x \sin\theta. \qquad (2)$$

The analysis uses an iterative least-squares fit to optimize seven parameters: peak density, 1/e width, ellipticity, vertical offset, and the amplitude, frequency, and phase of the oscillating column.

Plasma position detector (PPD): This instrument is mounted on the magnetic ramp leading to the high field coil at the north end of the central cell. Eight chords of plasma light are imaged onto an array of photomultipliers. A bandpass filter selects near-UV continuum light at 3435$\mathring{A}$ for observation, so that the signal is representative of the plasma temperature and density evolution. Gaussian fits are made to the PPD profiles and the plasma centroid and width calculated.

Endwall Faraday cup arrays: A linear array of Faraday cups extends across the narrow dimension of the fan at either end of the machine. The fans (which result from the plasma mapping out of the quadrupole anchors), and hence the Faraday cup arrays, are rotated at 90° with respect to each other. The cups have a negative bias to repel electrons and thus measure the ion endloss. Since the plasma is fueled from the central cell, all data presented in this paper will refer the Faraday cup physical positions to central cell well coordinates. The endwall data usually fits well to a Gaussian profile so that the centroid position of each array can be easily followed. The south end array represents motion in the up/down direction, while the north end array measures plasma motion in the east/west direction.

III. Structure and Evolution of the Instability

It is instructive to first consider the nature of the plasma after the instability has evolved to a saturated state. In Figure 3 we show the signals from four interferometers in the central cell array looking at -6, -4, 0, and 14 *cm* chord radii, (recall that the gas box limiter maps to 19.5 *cm* at the location of the interferometer array). We note three

salient features. (1) The plasma fluctuation remains coherent although the fluctuation in this case is quite severe. (2) There is no evidence for filamentation into irregular smaller structures. (3) The plasma executes a motion which is approximately periodic. The extent of the oscillation can be judged qualitatively from the fact that the plasma produces a double hump on the -6 *cm* chord, indicating that the center of the plasma column has passed through this chord.

In order to analyze the instability more quantitatively, we overlay on the experimental data in Figure 3 the results of a model in which we analyze the signals from the interferometer chords as if the plasma were an elliptic column with a Gaussian density profile. The column is assumed to co-rotate about its center as the plasma column oscillates about the machine axis, so that one axis of the ellipse is always oriented along a radial line from the axis of the machine. The parameters of the model are chosen to minimize the least squares error between the predicted values of the interferometer signals and the measured values over the time interval shown. We find an e-folding radius of 11.2 *cm* and an ellipticity of 1.08 . The center of the column oscillates in a circle of radius 6.2 *cm*. A comparison to the data shows that the

model is reasonably accurate. The model also predicts a vertical offset of the axis of rotation of -0.8 cm. Of course, the array can not resolve similar offsets in the horizontal direction. Note that the ellipticity is small indicating a circular plasma column even during these large amplitude oscillations.

In the analysis above we assumed the plasma column to have a Gaussian radial density profile. Although it might be possible that enhanced internal radial transport during the instability would lead the plasma to have a flatter core and steeper edges, we find that assuming a Gaussian profile yields a fit that is better qualitatively and has a lower value of chi^2. This is true both during quiescent and unstable operation at all but the highest gas fueling rates. In Figure 4 we show the results of an analysis in which we compare a Gaussian, a parabolic profile and a sharp edged profile, $n_e = 1 - (r/r_p)^8$. The density profiles as a function of radius are given for reference in Figure 4a. In Figure 4b we show the line densities that an observer would measure if he displaced the interferometer chords sinusoidally with the same frequency and amplitude as the plasma column. The data points are obtained by removing the sinusoidal oscillation from the data using

the best fit parameters for the oscillation amplitude and frequency. Qualitatively the Gaussian profile gives the best fit. This is confirmed by the chi^2 values for the fits which are also displayed in Figure 4a.

We can confirm our assumption that the plasma remains internally rigid while it oscillates about the machine axis by examining the Faraday cup signals. Referring to Figure 5, we have used one of the outermost Faraday cups as a reference signal and done a cross-correlation of this signal with the other signals in the same array. We have plotted the phase relative to the reference cup (plus 90° to make the plot symmetric about zero). We see that all the cups on the same side of the axis of rotation as the reference cup have a relative phase of 90°, while all cups on the opposite side from the reference have a relative phase of −90°. If the plasma column were asymmetric about a line passing through the machine axis, as for example an ellipse whose axis of symmetry did not intersect the machine axis, or a radially sheared profile such is commonly seen in theta pinches, the relative phases would have a very different structure. The mode, as seen in the endloss profile, is thus radially rigid, with the outer edge of the plasma strongly coupled to the interior.

We now examine our assumption that the plasma column oscillation about the machine axis is circular. Because the Faraday cup arrays are oriented at 90° to each other, we can plot the centroid of the endloss at each point in time, assuming that the end-loss profile is an off-center Gaussian. The y-axis is determined from the south array and the x-axis from the north array. Figure 6 shows the trajectory of the plasma column after the instability has saturated at a finite amplitude. The points along the trajectory are separated by 20 $\mu sec.$ The arrows indicate that the direction of travel of the plasma column is in the $\mathbf{E} \times \mathbf{B}$ direction, assuming a positive potential profile peaked on the machine axis. It is clear from this plot that the trajectory is not a perfect circle. The data shown are in fact an intermediate case, as some data indicate quite regular circular motion, while other data indicate a more elongated trajectory. We feel, however, that in general our model is very good at resolving the major aspects of the plasma motion.

We now investigate axial structure of the mode by examining in more detail data from the interferometer, PPD, and the endwall Faraday cup arrays. We again model the plasma at each of these axial

locations as a circular Gaussian column not necessarily centered on the machine axis. In Figure 7 we show the results from this analysis in which we have plotted the time history of the central peak from each of the arrays. All positions are referred back to the central cell well. Note the remarkable similarity of all three plots. Even though the detector locations cover essentially the entire machine length, we find each part of the machine is oscillating with the same fluctuation amplitude once magnetic field mapping corrections are made. We see no evidence for a trapped particle mode in Tara. In Figure 8 we show the cross-spectral analysis of the north and south Faraday cup centroids. From this plot we are able to read off directly the relative phase of the mode at each end of the machine. Note that this phase is very close to 90°; the angular separation of the arrays. Thus we conclude that the axial wavelength of the mode is many times the length of the machine. Assuming an error of ± 1 clock cycle in the measurement, we can place a lower bound on the axial wavelength of approximately 300 meters (with a 50 kHz clock). The Tara experiment is 25 meters long.

In the data presented thus far, the displacement of the plasma column has saturated at a finite amplitude. This is not always the case.

We show in Figure 9 the Faraday cup centroid trajectory immediately after the gyrotron power was applied. For the first 280 μsec after the pulse is initiated we see that the plasma does not move far from the machine axis. The motion up to this point is the same as seen before the gyrotron pulse. Then in approximately 160 to 200 μsec the displacement grows to an amplitude of 10 cm and leaves the view of the Faraday cup array where it presumably intersects a metal limiter in the central cell. We find that in cases of extreme instability, the mode amplitude can grow within one rotation time to the limiter radius, dumping the plasma (typically 100 to 300 $\mu secs$).

IV. Discussion and summary

Using information from an interferometer array, a light emission array detector and endwall Faraday cups, it is possible to characterize in a precise fashion the M=1 instability as seen in the Tara machine. We summarize the salient features of this instability: the mode is an axially rigid, periodic, coherent motion of the entire plasma column in which the column remains circular with a Gaussian density profile. The center of the column traces out a path that is approximately cir-

cular and centered on the machine axis. There is no evidence for filamentation of the plasma column or for trapped particle modes.

The coherence of the plasma column is remarkable considering the large departure from its quiescent state centered on the machine axis. We speculate that the coherence of the plasma column arises from ion Larmor radius effects. Bulk motions of the plasma across magnetic field lines must be quasi-neutral. However, since both electrons and ions $\mathbf{E}\times\mathbf{B}$ drift across field lines at the same velocity, to lowest order, no net perturbed charge is created during a motion of the plasma column. The dynamics of the motion are therefore determined by the requirement that the net charge vanish at higher order. The higher order sources of net charge are field line curvature, ion Larmor radius effects and ion polarization drifts. If the mode is not sufficiently rigid, the ion Larmor radius effects dominate and stabilize small perturbations from a centered equilibrium[21,22].

In Tara, the instability generally saturates at finite amplitude rather than growing until the plasma is lost to the chamber walls. Nevertheless, we conjecture that finite Larmor radius effects which force a mode to be rigid in the linear growth stage remain strong once the mode

has reached saturation. Similarly, such effects will also damp higher order modes as evidenced by the lack of deformation of the plasma column even during large amplitude oscillations.

This argument suggests that the dominance of finite Larmor radius effects which may account for the coherence of the mode in its saturated state may also account for the stability of the mode for operating parameters under which the plasma is observed to be quiescent. Specifically, stabilization mechanisms which stabilize the edge of the plasma such as the magnetic divertor or ponderomotive effects which may peak at the plasma surface, are able to stabilize the core of the plasma as well as the edge because of the rigidity induced by finite Larmor radius effects.

Acknowledgments:

We wish to thank Marcel Gaudreau and John Tarrh for their help in every aspect of Tara operation and engineering. We would also like to thank Wayne Brooks, Ken George, Richard Rameriz, Bill Stein, Paul Thomas, and Fee Yee for their technical support. Without their continuous help none of the data reported here could have been collected. This work was supported by the Department of Energy under contract number DE-AC02-78ET51013.

List of Figures:

1. A schematic of the Tara experiment showing the central slot antenna, gas box, and magnetic field geometry

2. Several important parameter time histories including (a) central cell density, (b) north plug gyrotron power, (c) central cell diamagnetism, and (d) central cell density

3. We display four interferometer signals during a large amplitude instability. During part of the trace, we have overlaid the results of a simulation in which the plasma profile is assumed to be Gaussian and rotating 6.2 *cm* off the machine axis. The remaining parameters of the model, which are chosen to minimize the least squares error, are: central density of 2.e12, plasma 1/e radius of 11.2 cm, frequency of rotation of 3 kHz, vertical off-set of oscillation center of .8 cm, and ellipticity of 1.08. The chi-squared value for this fit was 1.2. Note the close correlation between the simulated and actual data.

4. Several model radial profiles were tried in order to determine which one gave the best fit. We find that a Gaussian profile is the best fit to the data. (a) Line integrated density profiles vs. chord radius

for the Gaussian, parabolic, and sharp edged model density profiles are shown for reference. The data points are the average for several cycles of the interferometer signals at the time when the center of the plasma column passes through the on-axis interferometer arm. The error bars represent the cycle to cycle variation of the density. (b) The density profiles used in the model.

5. Using the outermost Faraday cup as a reference, we have plotted the relative phase of the other cups in the array during the instability. There is very little shear across the plasma profile. The edge of the plasma column is very rigidly coupled to the core.

6. We plot the trajectory of the plasma column as determined by the Faraday cup arrays. In this plot we show the growth of the M=1 mode from a quiescent state to one with a 10 cm mode amplitude. Growth times of 100-200 μsec are indicated. The time between data points is 20 μsec.

7. The Faraday cups, PPD, and interferometer array all provide information about the vertical position of the plasma column. We show here the location of the plasma centroid as measured by these

three diagnostics. All positions are mapped to the central cell well. These data indicate very clearly that the mode amplitude is constant throughout the machine.

8. The Faraday cup arrays at each end of the machine are rotated 90° with respect to each other. By measuring the relative phase of the endwall wall centroids we see that the parallel wavelength of the mode is very long; much longer than the machine length.

9. The centroid information from each end of the machine is used to follow the plasma column during the instability. The time between data points is 20 μsec. We are able to follow the plasma from an early quiescent phase, through the instability growth phase, and finally into a plasma dump.

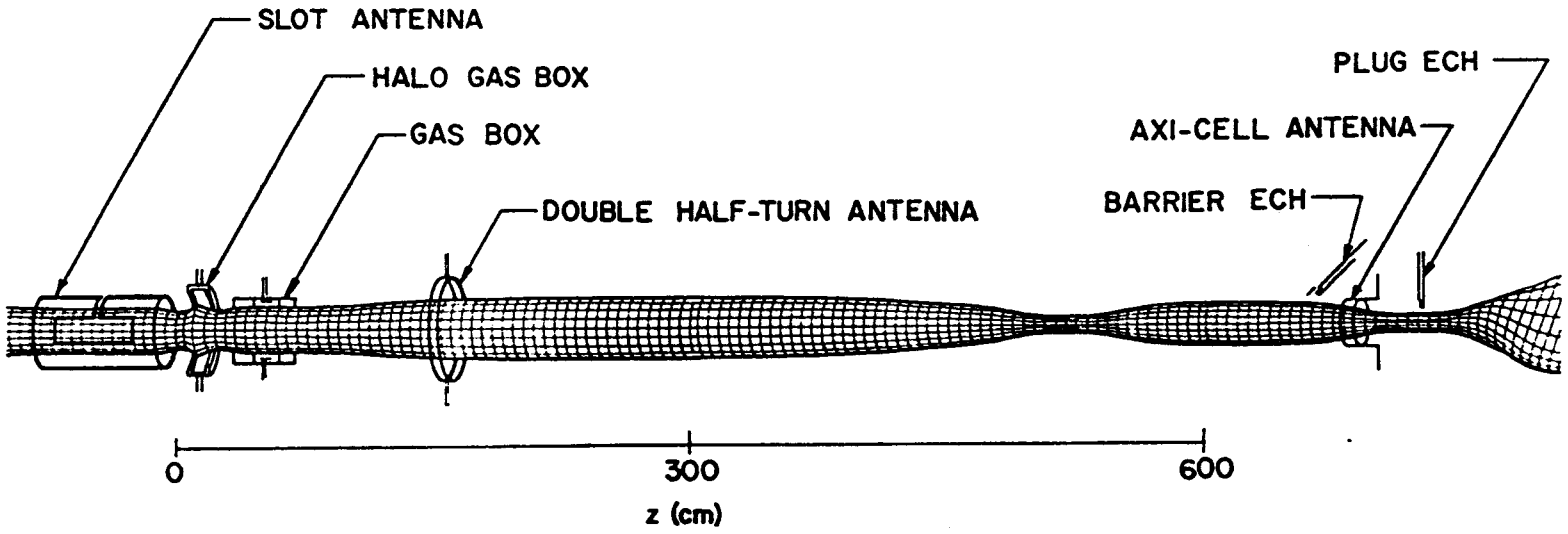

TARA MAGNETIC FIELD GEOMETRY

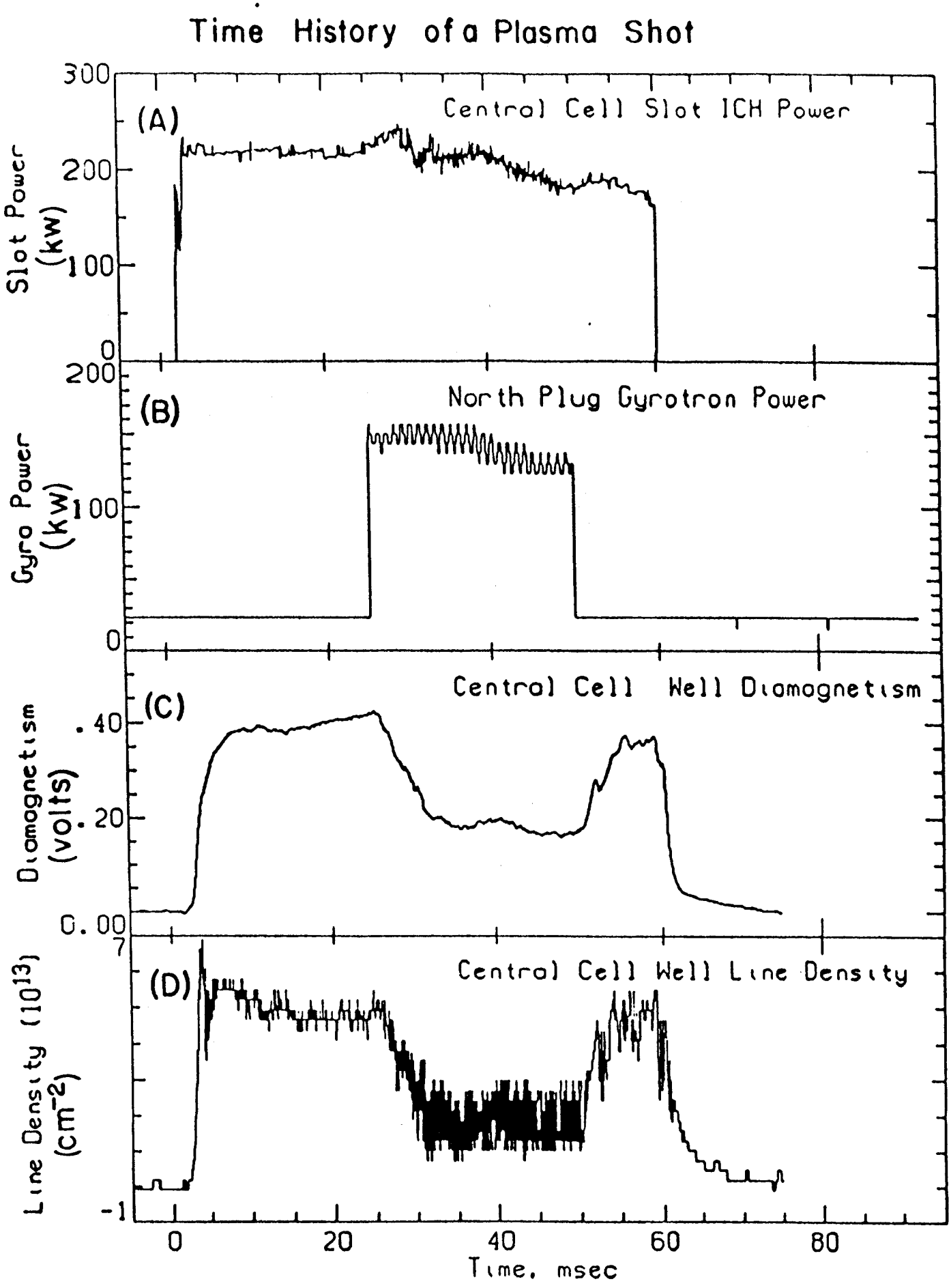
Time History of a Plasma Shot
(A)
Central Cell Slot ICH Power
Slot Power (kw)
300
200
100
0
(B)
North Plug Gyrotron Power
Gyro Power (kw)
200
100
0
(C)
Central Cell Well Diamagnetism
Diamagnetism (volts)
.40
.20
0.00
(D)
Central Cell Well Line Density
Line Density (10^{13}) (cm^{-2})
7
-1
0
20
40
60
80
Time, msec

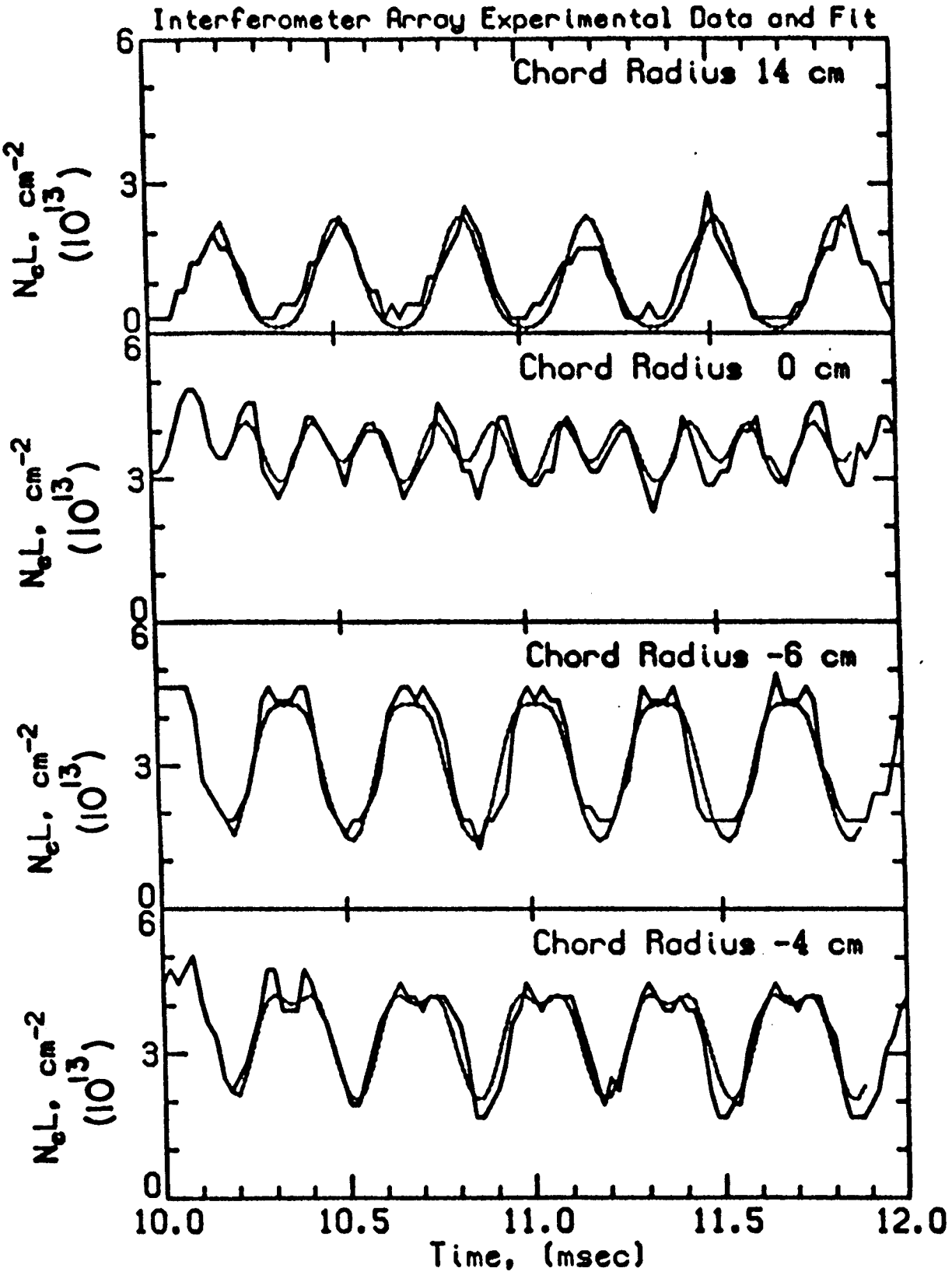
Interferometer Array Experimental Data and Fit
Chord Radius 14 cm
Chord Radius 0 cm
Chord Radius -6 cm
Chord Radius -4 cm
N_eL, cm^{-2} (10^{13})
6
3
0
10.0
10.5
11.0
11.5
12.0
Time, (msec)

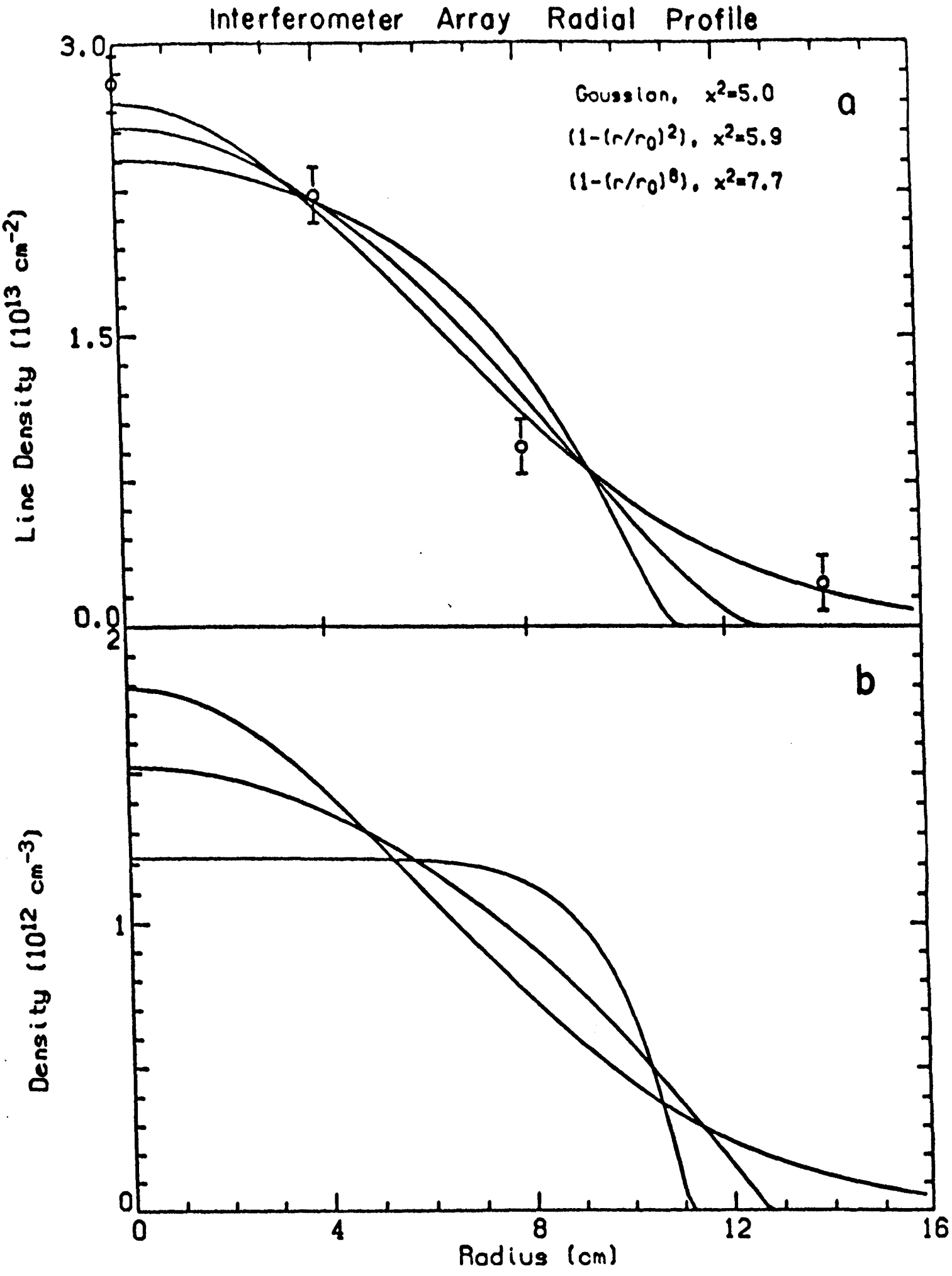
Interferometer Array Radial Profile
Gousslon, x^2=5.0
$(1-(r/r_0)^2)$, x^2=5.9
$(1-(r/r_0)^8)$, x^2=7.7
a
b
Line Density (10^{13} cm^{-2})
Density (10^{12} cm^{-3})
Radius (cm)
3.0
1.5
0.0
2
1
0
0
4
8
12
16

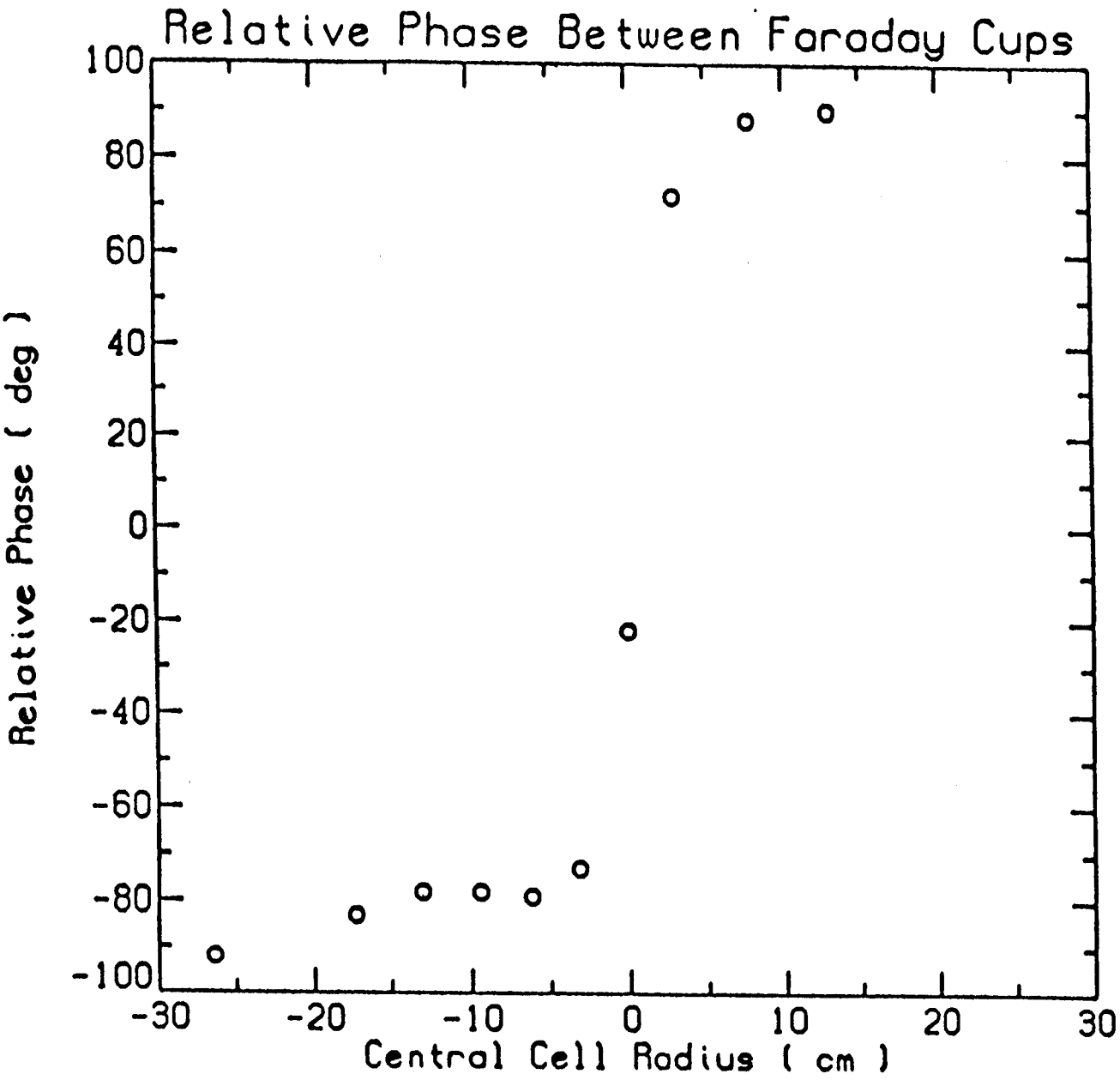
Relative Phase Between Faraday Cups
Relative Phase (deg)
100
80
60
40
20
0
-20
-40
-60
-80
-100
-30
-20
-10
0
10
20
30
Central Cell Radius (cm)

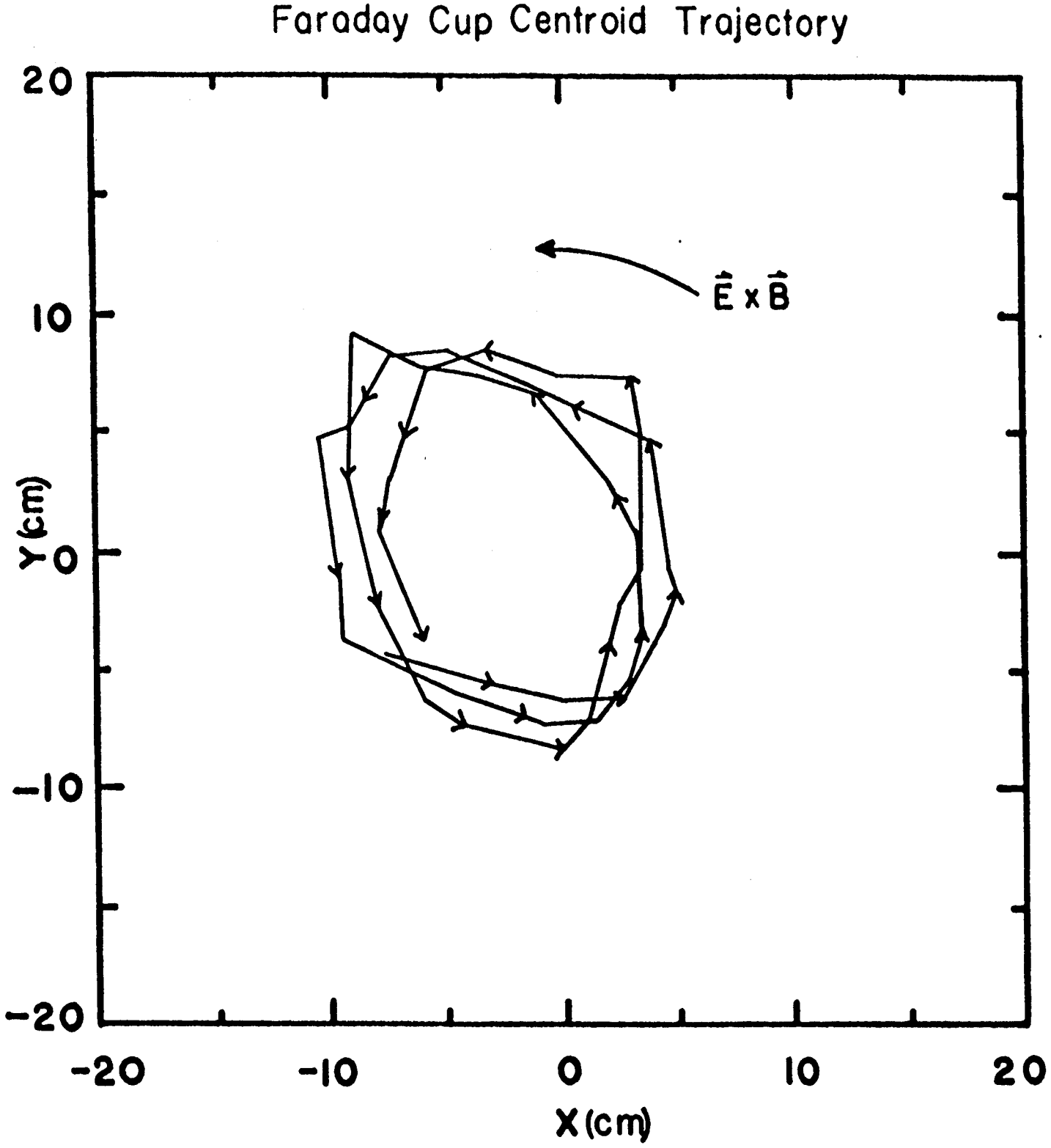
Faraday Cup Centroid Trajectory
20
10
0
-10
-20
Y(cm)
-20
-10
0
10
20
X(cm)
$\hat{E} \times \hat{B}$

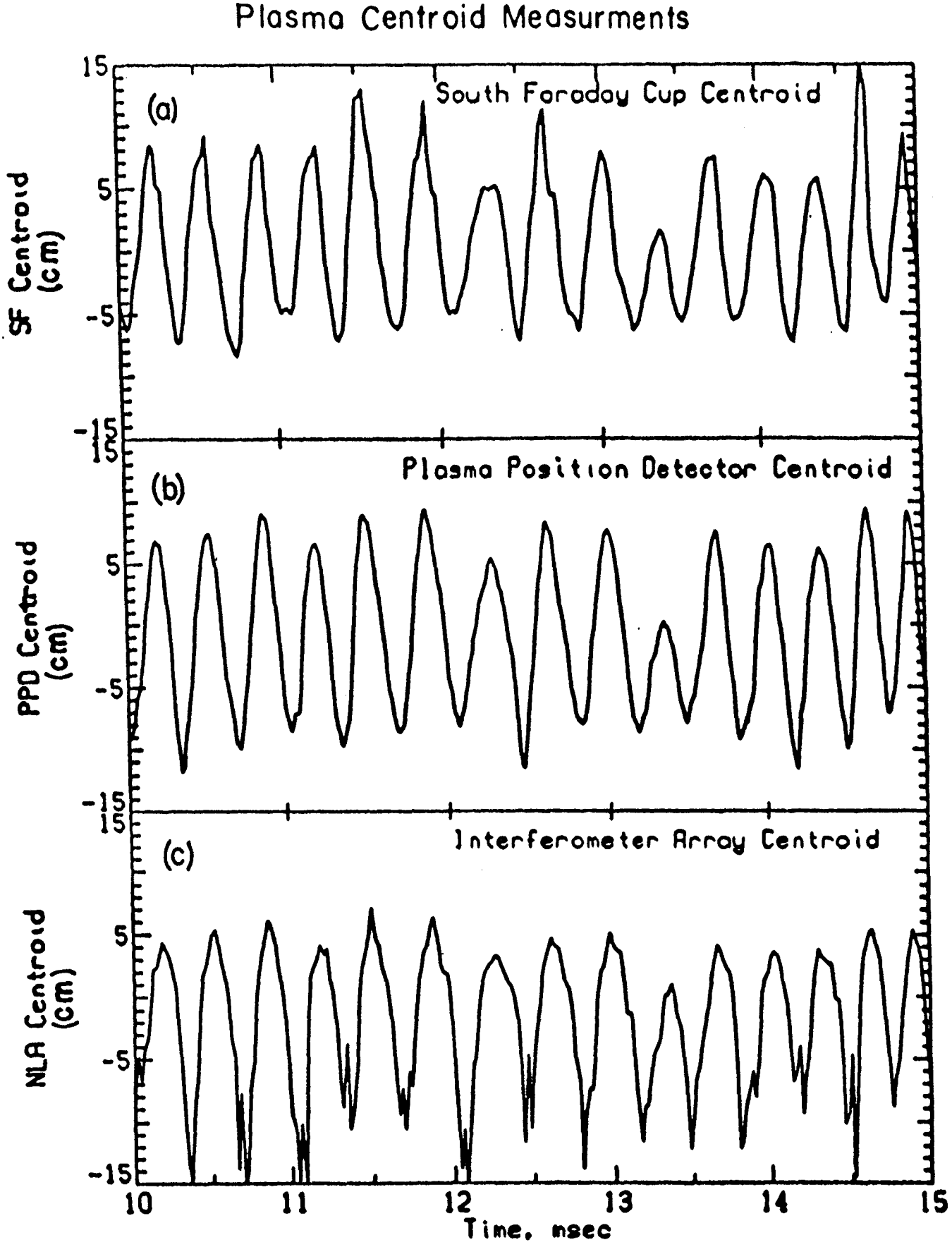
Plasma Centroid Measurments
(a)
South Foraday Cup Centroid
SF Centroid (cm)
15
5
-5
-15
(b)
Plasma Position Detector Centroid
PPD Centroid (cm)
15
5
-5
-15
(c)
Interferometer Array Centroid
NLA Centroid (cm)
15
5
-5
-15
10
11
12
13
14
15
Time, msec

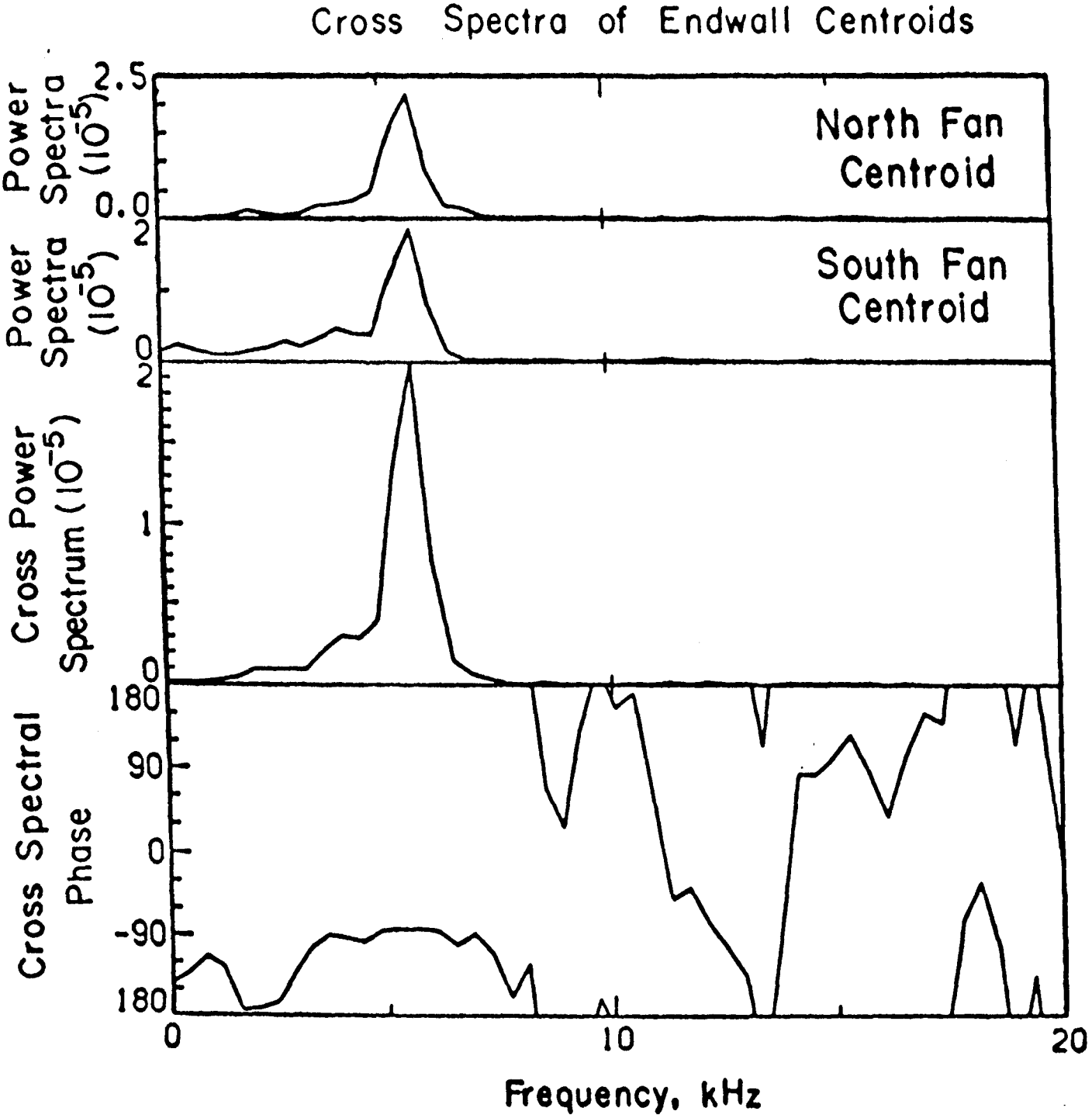
Cross Spectra of Endwall Centroids
Power Spectra (10^{-5})
2.5
0.0
North Fan Centroid
Power Spectra (10^{-5})
2
0
South Fan Centroid
Cross Power Spectrum (10^{-5})
2
1
0
Cross Spectral Phase
180
90
0
-90
180
0
10
20
Frequency, kHz

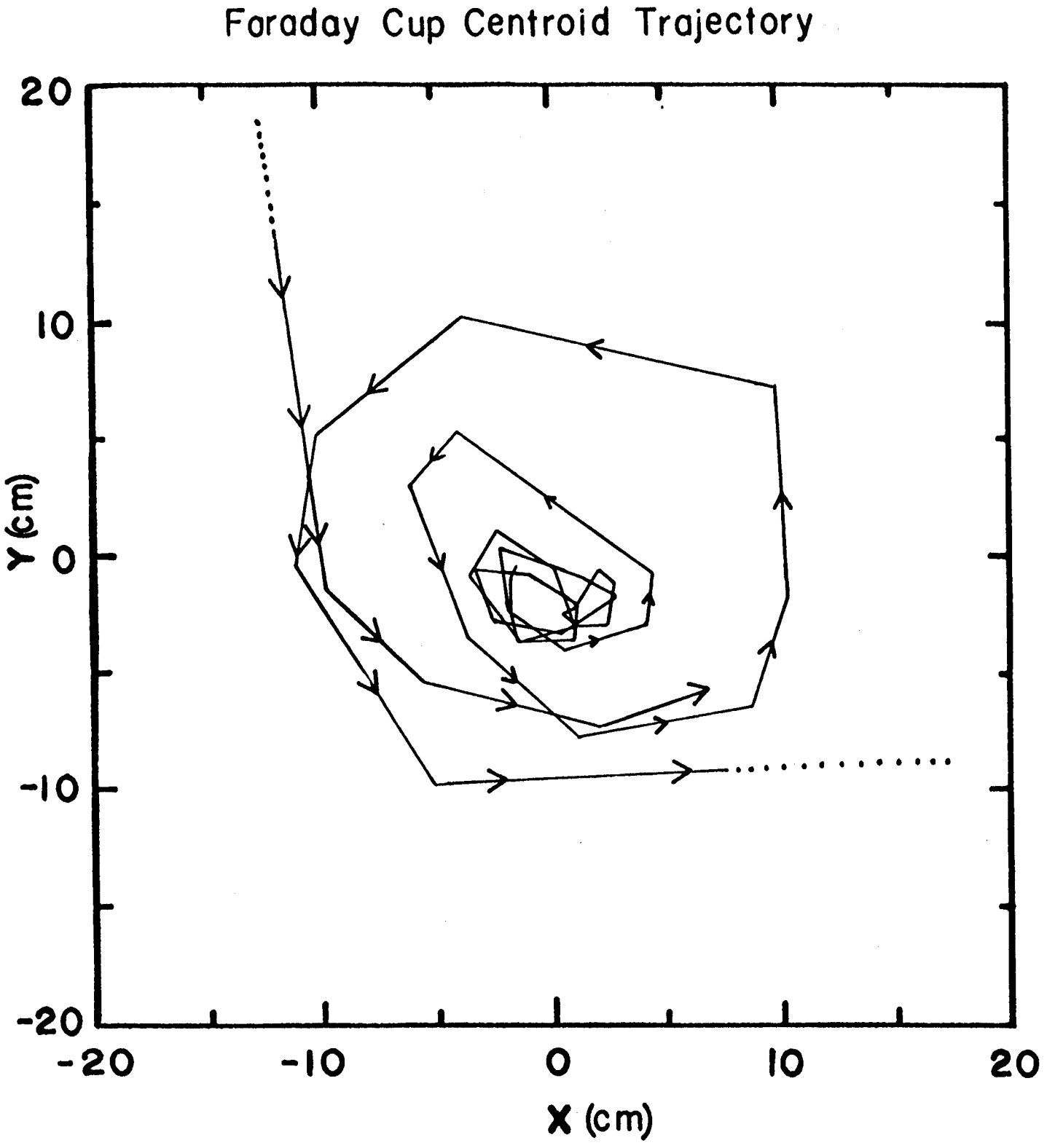
Faraday Cup Centroid Trajectory
20
10
0
-10
-20
Y (cm)
-20
-10
0
10
20
X (cm)

References

[1] J. Kesner, R.S. Post, B. D. McVey, D.K. Smith, Nucl. Fus. **22**, 549 (1982).

[2] R.S. Post et al., International Conference on Plasma Physics and Controlled Nuclear Fusion Research, **2**, 285 (IAEA) London, (1985).

[3] Hooper et al., Nucl. Fus. **22**, 549 (1982).

[4] Ferron et al., to be published Phys. Fl., June 1987

[5] Molvik et al., Phys. Fl. **27**, 2711 (1984).

[6] Molvik et al., Phys. Rev. Lett. **48**, 742 (1982).

[7] R. Itatani, H. Takeno, Y. Yasaka, Eleventh International Conference on Plasma Physics and Controlled Nuclear Fusion Research, Kyoto, IAEA-CN-47/C-I-4-2, (1986).

[8] M.S. Ioffe, R.I. Sobolev, V.G. Telkovskii, E.E. Yushmanov, Sov. Phys. J.E.T.P. **12**, 1117 (1961).

[9] W.A. Perkins, R.F. Post, Phys. Fl. **6**, 1537 (1963).

[10] K. Brau, P. Goodrich, R.S. Post, E. Sevillano, J. Vac. Sci. Technol. **A 4**, 1079 (1986).

[11] J.R. Ferron, N. Hershkowitz, R.A. Breun, S.N. Golovato, and R. Goulding, Phys. Rev. Lett. **51**, 1955 (1983).

[12] Y. Yasaka and R. Itatani, Nucl. Fus. **24**, 445 (1984).

[13] H. Akimune, I. Ikeda, T. Hirata, and F. Okamoto, J. Phys. Soc. Jpn. **50**, 2729 (1981).

[14] J.R. Myra and D.A. D'Ipposlito, Phys. Rev. Lett. **53**, 914 (1984).

[15] D.A. D'Ippolito and J.R. Myra, Phys. Fl. **29**, 2594 (1986).

[16] J.B. McBride, V. Stefan, and N.A. Krall, Phs. Rev. Lett. **54**, 42 (1985).

[17] P.L. Similon and A.N. Kaufman, Phys. Rev. Lett. **53**, 1061 (1984).

[18] B.I. Cohen and T.D. Rognlien, Phys. Fl. **28**, 2194 (1985).

[19] M.J. Gerver and B. Lane, Phys. Fl. **29**,2214 (1986).

[20] Magnetic Divertor paper in preparation

[21] M.N. Rosenbluth, N.A. Krall, N. Rostoker, Nucl Fusion Suppl., Pt. 1,143 (1962).

[22] M.N. Rosenbluth and A. Simon, Phys. Fl. **8**, 1300 (1965).